Original Article

Institution of MECHANICAL ENGINEERS
Journal of MECHANICAL ENGINEERING SCIENCE

Proc IMechE Part C:
J Mechanical Engineering Science
2016, Vol. 230(11) 1921–1936

DOI: 10.1177/0954406215586232
pic.sagepub.com
SAGE

Magnetic field effects on the slip velocity and temperature jump of nanofluid forced convection in a microchannel

Arash Karimipour and Masoud Afrand

Abstract

Forced convection of water–Cu nanofluid in a two-dimensional microchannel is studied numerically. The microchannel wall is divided into three parts. The entry and exit ones are kept insulated while the middle one has more temperature than the inlet fluid. The whole of microchannel is under the influence of a magnetic field with uniform strength of B_0. Slip velocity and temperature jump are involved along the microchannel walls for different values of slip coefficient such as $B = 0.001$, $B = 0.01$, and $B = 0.1$ for $Re = 10$, $Re = 50$, and $Re = 100$. Navier–Stokes equations are discretized and numerically solved by a developed computer code in FORTRAN. Results are presented as the velocity, temperature, and Nusselt number profiles. Moreover, the effect of magnetic field on slip velocity and temperature jump is investigated for the first time in the present work. Larger Hartmann number, Reynolds number, and volume fraction correspond to more heat transfer rate; however, the effects of Ha and φ are more significant at higher Re.

Keywords

Nanofluid, magnetic field, microchannel, slip velocity, temperature jump

Date received: 25 April 2014; accepted: 23 March 2015

Introduction

Convection heat transfer mechanism is the only significant way of heat transfer in conventional fluids like water due to their low thermal conductivity. However, increasing the fluid conductivity could be an alternative method to enhance the heat transfer rate. The well-known innovative way to increase the fluid thermal conductivity is to suspend the nanoparticles of a solid in a base fluid. The mixture obtained has higher thermal conductivity than that of the base fluid which is called nanofluid.[1–3] A review of nanofluid performance at different physical geometries is presented as follows: at first, the simulation of nanofluid free and forced convection in the cavities and enclosures are reported. Later several works concerning nanofluid flow in tubes and ducts are presented.

A number of studies regarding the fluid flow and heat transfer of nanofluid in different physical conditions[4–7] such as the simulation of nanofluid free convection in a rectangular cavity was reported by Oztop and Abu-Nada.[8] They used different types of nanoparticles such as TiO_2, Cu, AL_2O_3 in their work. Moreover, several researchers tried to investigate the nanofluid performance in other domains; among them Tiwari and Das[9] showed the positive effect of Copper–water nanofluid to increase Nusselt number in a two-sided lid-driven enclosure. More works can be referred to concerning nanofluid mixed convection in cavities.[10–13] Simulation of nanofluid flow in ducts or tubes are also other attractive topics for researchers. Fully developed nanofluid mixed convection in a horizontal curved pipe was studied by Akbarinia and Behzadmehr.[14] In several other works, different aspects of nanofluid flow such as consideration of the nanofluid mixture as a two-phase substance or turbulence forced convection of nanofluid were investigated.[15–18] Present work aims to simulate a microflow through a microchannel. Fluid flow and heat transfer at microscales are different from macroscales level, as a result a succinct description of a microchannel flow is presented in below.

In recent years, much attention has been paid to the development of the performance of micro-devices. Appropriate efficiency besides their small scale are some of the advantages of these instruments which have a large application these days.[19–23] The surface

Department of Mechanical Engineering, Najafabad Branch, Islamic Azad University, Isfahan, Iran

Corresponding author:
Arash Karimipour, Department of Mechanical Engineering, Najafabad Branch, Islamic Azad University, Isfahan, Iran.
Email: arashkarimipour@gmail.com

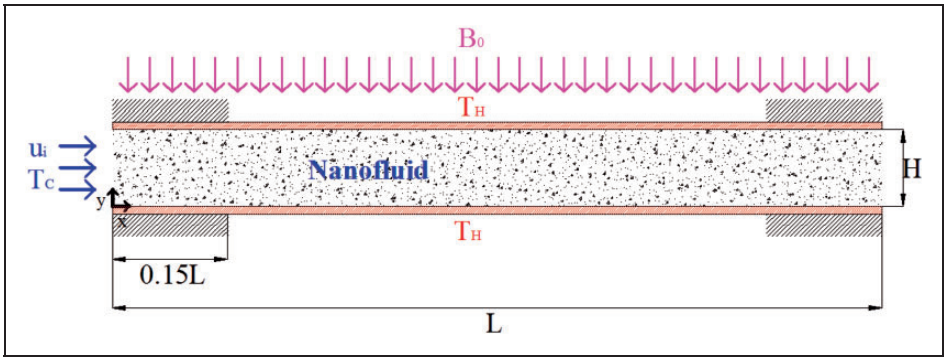

Figure 1. The microchannel physical configuration.

effects are more important at microscales level than the usual metric ones. As a result for a micro-liquid flow, the classic no-slip boundary condition is dropped and slip flow regimes involving slip velocity and temperature jump should be considered along the boundaries. However, other flow regimes such as slip, transient, and free molecular ones are introduced for the micro-gas flows. At these levels, the particle base approaches like lattice Boltzmann method or molecular dynamic can be applied.[24–28] The nanofluid performance at different geometries besides the properties of micro-flow was reported. The combination of both last cases could be an innovative approach to increase the heat transfer from the microchannel walls. This means more efficiency can be achieved by using nanofluid flow in a microchannel, which has been reported by several studies as follows.

Raisi et al.[29] studied nanofluid flow in a microchannel in both slip and no-slip boundary conditions and computed the averaged Nusselt number for both these conditions. A number of studies concerning the nanofluid flow and heat transfer through a microchannel can be referred to.[30–36] As a follow-up study, some researchers tried to investigate the influence of a magnetic field on the flow domain. Hence, a brief review regarding the MHD flow is presented in the next section.

In several practical cases like magneto-hydrodynamic flows (MHD), the flow of electrically conducting fluid through a channel occurs in the presence of a transverse magnetic field. The influence of this magnetic field would generate a force, called Lorentz force, which affects the flow domain.[37–41]

It was observed that the slip velocity and temperature jump were ignored in a previous work, which studied the MHD nanofluid flow in a microchannel.[42] However, what distinguishes the present article from the previous ones is the investigation of the effects of magnetic field on slip velocity and temperature jump of nanofluid in a microchannel. To the best of authors' knowledge, the effect of magnetic field on nanofluid's slip velocity and temperature jump has been ignored in previous works owing to which it has been studied for the first time in the present work.

Problem statement

Forced convection of water–Cu nanofluid in a two-dimensional horizontal microchannel is studied numerically. Microchannel aspect ratio (AR) is high enough as $AR = L/H = 20$, so the fully developed condition is achieved at outlet. The microchannel wall is divided into three parts. The entry and exit ones are kept insulated while the middle one has more temperature than the inlet fluid (Figure 1). Moreover, the whole of microchannel is under the influence of a magnetic field with uniform strength of B_0.

Nanofluid Reynolds number (Re) usually has a small value in a microchannel duo to express a real physical condition, so the inlet Re is considered as $Re = 10$, $Re = 50$, and $Re = 100$. In addition, slip velocity and temperature jump boundary conditions are involved along the microchannel walls for different values of slip coefficient such as $B = 0.001$, $B = 0.01$, and $B = 0.1$. Three different amounts of nanoparticle volume fractions such as $\varphi = 0$, $\varphi = 0.02 = 2\%$, and $\varphi = 0.04 = 4\%$ are applied. It is supposed that nanofluid is incompressible Newtonian homogeneous mixture. Moreover, the diameter of spherical nanoparticles is $d_p = 10\,\text{nm}$ and radiation effects are negligible.

Numerical procedure

Governing equations

Two-dimensional Cartesian Navier–Stokes equations for nanofluid are given as follows[43]

Continuity

$$\frac{\partial u}{\partial x} + \frac{\partial v}{\partial y} = 0 \tag{1}$$

X-momentum

$$u\frac{\partial u}{\partial x} + v\frac{\partial u}{\partial y} = -\frac{1}{\rho_{nf}}\frac{\partial p}{\partial x} + \upsilon_{nf}\left(\frac{\partial^2 u}{\partial x^2} + \frac{\partial^2 u}{\partial y^2}\right) - \frac{\sigma_{nf}B_0^2}{\rho_{nf}}u \tag{2}$$

Y-momentum

$$u\frac{\partial v}{\partial x}+v\frac{\partial v}{\partial y}=-\frac{1}{\rho_{nf}}\frac{\partial p}{\partial y}+\upsilon_{nf}\left(\frac{\partial^2 v}{\partial x^2}+\frac{\partial^2 v}{\partial y^2}\right) \tag{3}$$

Energy

$$u\frac{\partial T}{\partial x}+v\frac{\partial T}{\partial y}=\alpha_{nf}\left(\frac{\partial^2 T}{\partial x^2}+\frac{\partial^2 T}{\partial y^2}\right) \tag{4}$$

Nanofluid characteristics can be determined according to thermophysical properties of fluid and nanoparticles, such as density and viscosity

$$\rho_{nf}=\varphi\rho_s+(1-\varphi)\rho_f \tag{5}$$

$$\mu_{nf}=\mu_f/(1-\varphi)^{2.5} \tag{6}$$

Subscript f is applied for the base fluid, s for solid nanoparticles, and nf for nanofluid.

Now, heat capacity is achieved by using equation (5) and Xuan and Li[44] formula

$$(\rho c_p)_{nf}=(1-\varphi)(\rho c_p)_f+\varphi(\rho c_p)_s \tag{7}$$

Effective nanofluid thermal conductivity is determined by Chon et al. model.[45] Brownian motions and diameter of nanoparticles can be taken into account in their model as

$$\frac{k_{eff}}{k_f}=1+64.7\times\varphi^{0.7460}\left(\frac{d_f}{d_p}\right)^{0.3690}\left(\frac{k_s}{k_f}\right)^{0.7476}\times\left(\frac{\mu}{\rho_f\alpha_f}\right)^{0.9955}\left(\frac{\rho_f B_c T}{3\pi\mu^2 l_{BF}}\right)^{1.2321} \tag{8}$$

where $l_{BF}\approx 0.17\,\text{nm}$ is the base fluid mean free path and $B_c=1.3807\times10^{-23}\,\text{J/K}$ is Boltzmann constant. Moreover μ is estimated as follows

$$\mu=A\left(10^{\frac{B}{T-C}}\right),\quad C=140(\text{K}),\quad \text{B}=247(\text{K}),\quad A=2.414(10^{-5})(\text{Pa.s}) \tag{9}$$

Nanofluid effective electrical conductivity is determined by Maxwell's model[43,46] as below

$$\frac{\sigma_{nf}}{\sigma_f}=1+\frac{3(\sigma_s/\sigma_f-1)\varphi}{(\sigma_s/\sigma_f+2)-(\sigma_s/\sigma_f-1)\varphi} \tag{10}$$

The following dimensionless variables are applied to approach dimensionless governing equations from equations (1) to (4)

$$H=h/h=1,\quad L=l/h=20$$
$$Y=y/h,\quad X=x/h$$
$$V=v/u_i,\quad U=u/u_i$$
$$\theta=(T-T_C)/(T_H-T_C)$$
$$P=p/(\rho_{nf}u_i^2) \tag{11}$$

Dimensionless continuity

$$\frac{\partial U}{\partial X}+\frac{\partial V}{\partial Y}=0 \tag{12}$$

Dimensionless X-momentum

$$U\frac{\partial U}{\partial X}+V\frac{\partial U}{\partial Y}=-\frac{\partial P}{\partial X}+\frac{1}{PrRe}\frac{\upsilon_{nf}}{\alpha_f}\left(\frac{\partial^2 U}{\partial X^2}+\frac{\partial^2 U}{\partial Y^2}\right)-\frac{Ha^2}{Re}\frac{\sigma_{nf}}{\sigma_f}\frac{\rho_f}{\rho_{nf}}U \tag{13}$$

Dimensionless Y-momentum

$$U\frac{\partial V}{\partial X}+V\frac{\partial V}{\partial Y}=-\frac{\partial P}{\partial Y}+\frac{1}{PrRe}\frac{\upsilon_{nf}}{\alpha_f}\left(\frac{\partial^2 V}{\partial X^2}+\frac{\partial^2 V}{\partial Y^2}\right) \tag{14}$$

Dimensionless energy

$$U\frac{\partial\theta}{\partial X}+V\frac{\partial\theta}{\partial Y}=\frac{\alpha_{nf}}{\alpha_f}\frac{1}{Re.Pr}\left(\frac{\partial^2\theta}{\partial X^2}+\frac{\partial^2\theta}{\partial Y^2}\right) \tag{15}$$

where $Re=u_i h/\upsilon_f$ and $Pr=\upsilon_f/\alpha_f$ and $Ha=B_0 h(\sigma_f/\mu_f)^{0.5}$.

In previous work which concerned nanofluid forced convection in microchannel, Hartmann number (Ha) was defined based on nanofluid properties.[42] However, Ha should be defined according to fluid properties to have consistency with definitions of Pr and Re; hence the last term in right-hand side of equation (13) is derived and presented here.

Hydrodynamic boundary conditions

L_s, u_{wall}, and u_{liquid} are introduced as the slip length, wall velocity, and liquid velocity on the wall to simulate the slip velocity as follows[47]

$$\Delta u_{wall}=u_{fluid}(y\to wall)-u_{wall}=L_s\left.\frac{\partial u_{fluid}(y)}{\partial y}\right|_{wall} \tag{16}$$

As a result, the nanofluid slip velocity (u_s) on the stationary walls can be achieved[48]

$$u_s=\pm\beta\left.\frac{\partial u}{\partial y}\right|_{y=0,h} \tag{17}$$

Table 1. Nu_m at different grids for $\varphi = 0.02$ and $\varphi = 0.04$ at $Re = 10$, $Ha = 0$, and $B = 0.001$.

	500×25	600×30	700×35
$\varphi = 0.02$	2.0526	2.0530	2.0532
$\varphi = 0.04$	2.1193	2.1200	2.1203

Table 2. The values of U and θ at the point of $X = L/2$ and $Y = 0.5$ at different grids for $\varphi = 0.04$, $Re = 10$, $Ha = 0$, and $B = 0.001$.

	500×25	600×30	700×35
U	1.498	1.499	1.499
θ	0.761	0.763	0.764

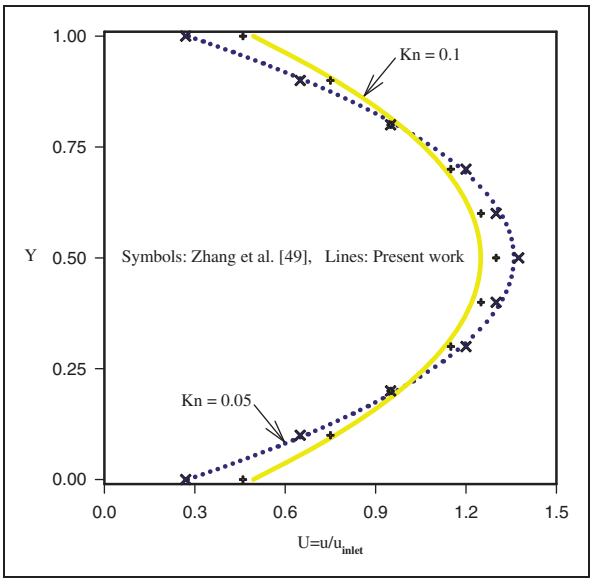

Figure 2. Comparison of present work's fully developed velocity profiles with those of Zhang et al.[49]

β indicates the slip coefficient. By showing equation (17) in dimensionless form, hydrodynamic boundary condition along the walls is derived as

$$U_s = \pm B \left. \frac{\partial U}{\partial Y} \right|_{Y=0,1} \tag{18}$$

where $B = \beta/h$ is the dimensionless slip coefficient.

Thermal boundary conditions

Temperature jump effects are considered in this study. Similar to equation (16), temperature jump can be simulated on the microchannel walls as follows[31]

$$\Delta T_{wall} = T_{fluid}(y \to wall) - T_{wall} = \zeta \left. \frac{\partial T_{fluid}(y)}{\partial y} \right|_{wall} \tag{19}$$

where ζ is the temperature jump distance. Consequently, dimensionless thermal boundary condition along the hot walls of microchannel for $0.15L < X < 0.85L$ is shown as

$$\theta - \theta_{wall} = \frac{B}{Pr} \left. \frac{\partial \theta}{\partial Y} \right|_{Y=0,1} \tag{20}$$

in which $\theta_{wall} = 1$. Equation (20) indicates the value of temperature jump as $\theta_s = abs(\theta - \theta_{wall})$.

Uniform cold flow is supposed for the inlet which in dimensionless form could be written as $U_i = 1$, $V_i = 0$, and $\theta_i = \theta_c = 0$. For the outlet, the fully developed hydrodynamic and thermal boundary conditions are considered as $V_{out} = 0$ and $\partial U_{out}/\partial X = \partial \theta_{out}/\partial X = 0$. Insulated walls at $0 < X < 0.15L$ and $0.85L < X < L$ are simulated by $\partial \theta/\partial Y = 0$ at $Y = 0$ and $Y = 1$.

Local and averaged Nusselt numbers (Nu_X and Nu_m) along the walls are demonstrated as follows

$$\begin{aligned} Nu_X)_{lower\ wall} &= -\frac{k_{eff}}{k_f} \left(\frac{\partial \theta}{\partial Y} \right)_{Y=0}, \\ Nu_X)_{upper\ wall} &= -\frac{k_{eff}}{k_f} \left(\frac{\partial \theta}{\partial Y} \right)_{Y=1} \end{aligned} \tag{21}$$

$$Nu_m = \frac{1}{0.7L} \int_{0.15L}^{0.85L} Nu_X \mathrm{d}X \tag{22}$$

Results and discussion

A computer code in FORTRAN language was developed to simulate the problem by the finite volume approach according to the SIMPLE algorithm. Discretization of the diffusion and convective terms were done by the *power law* and the implicit scheme was applied to deal with the time differential terms.

The convergence condition was achieved by convergence criterion $\varepsilon = 5 \times 10^{-7}$ greater than the related error, $((\Omega^{n+1} - \Omega^n)/\Omega^{n+1})$, for each variable of $\Omega = U$, V, and θ at each consecutive time step n and $n+1$; which led to $abs((\Omega^{n+1} - \Omega^n)/\Omega^{n+1}) < \varepsilon$.

Grid study and validation

Tables 1 and 2 show the averaged Nusselt number of nanofluid through the microchannel at different grids of 500×25, 600×30, and 700×35 for $\varphi = 0.02$ and $\varphi = 0.04$ at $Re = 10$, $Ha = 0$, and $B = 0.001$. It is seen that difference between those of 600×30 and 700×35 are negligible; as a result, grid nodes of 600×30 is selected for the next computations.

To validate the developed using code, results of present work versus those of Zhang et al.[49] are presented in Figure 2. In this figure, fully developed velocity profiles of the air flow through a microchannel for different values of Knudsen number

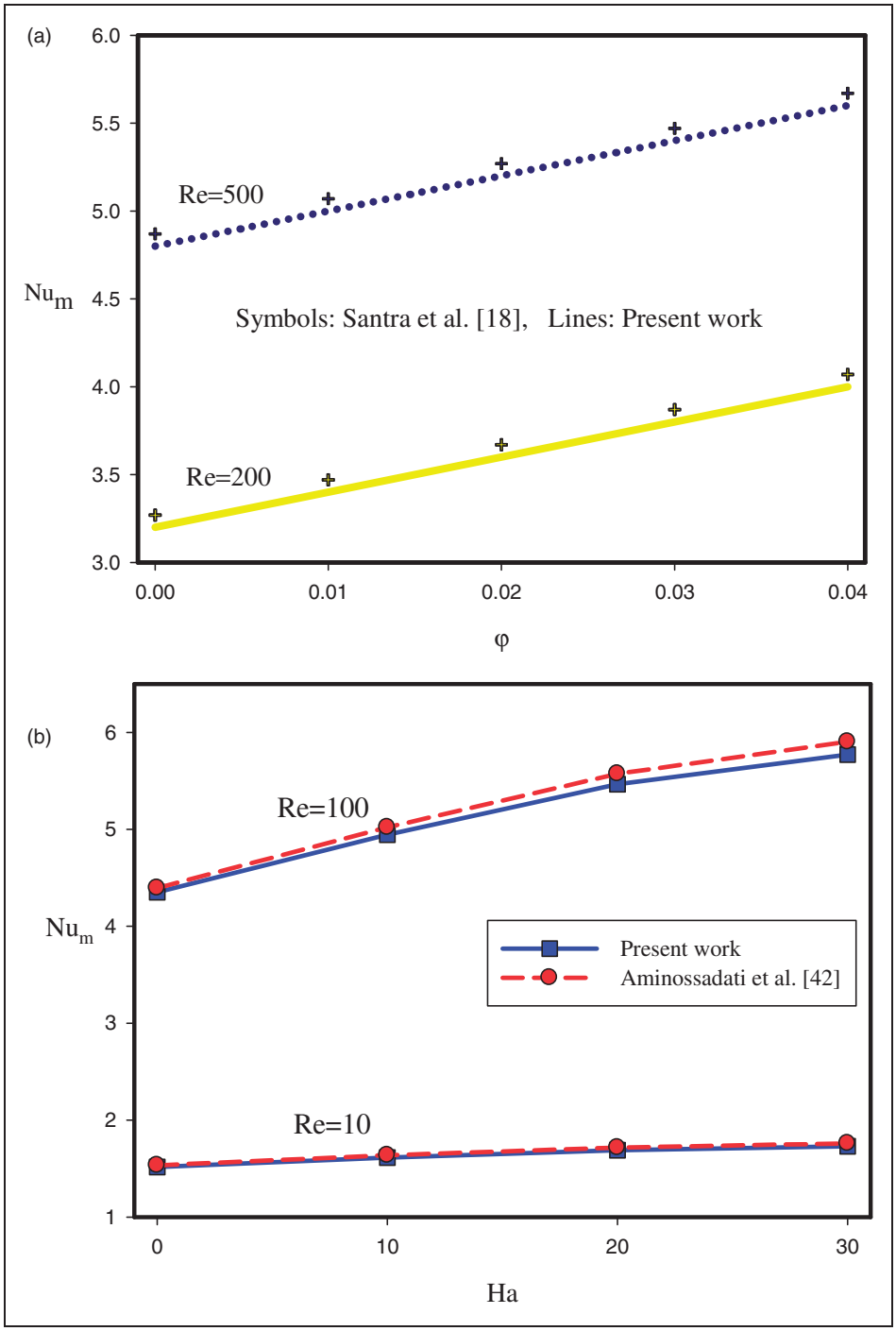

Figure 3. (a) Nu_m from present work versus Santra et al.[18] for different values of *Re* and φ; (b) Nu_m from present work versus Aminossadati et al.[42] for different values of *Re* and *Ha* at $\varphi = 0.02$.

(*Kn*) are compared. Moreover, averaged Nusselt number of nanofluid in a channel flow is compared with the results of Santra et al.[18] in Figure 3(a). The last selected case for validation would be a work of Aminossadati et al.[42] which is shown in Figure 3(b) and concerns a nanofluid forced convection flow in a microchannel under a magnetic field and in the absence of slip velocity. Appropriate agreements are seen in Figure 2, Figure 3(a) and (b).

Table 3. Thermo-physical properties of copper and water at 20°C.

	c_p (J/kgK)	ρ (kg/m^3)	K (W/mK)	μ (Pas)	σ (S/m)	*Pr*
Water	4182	998	0.6	1×10^{-3}	5.96×10^{7}	6.9
Cu	383	8960	401	–	5.0×10^{-2}	–

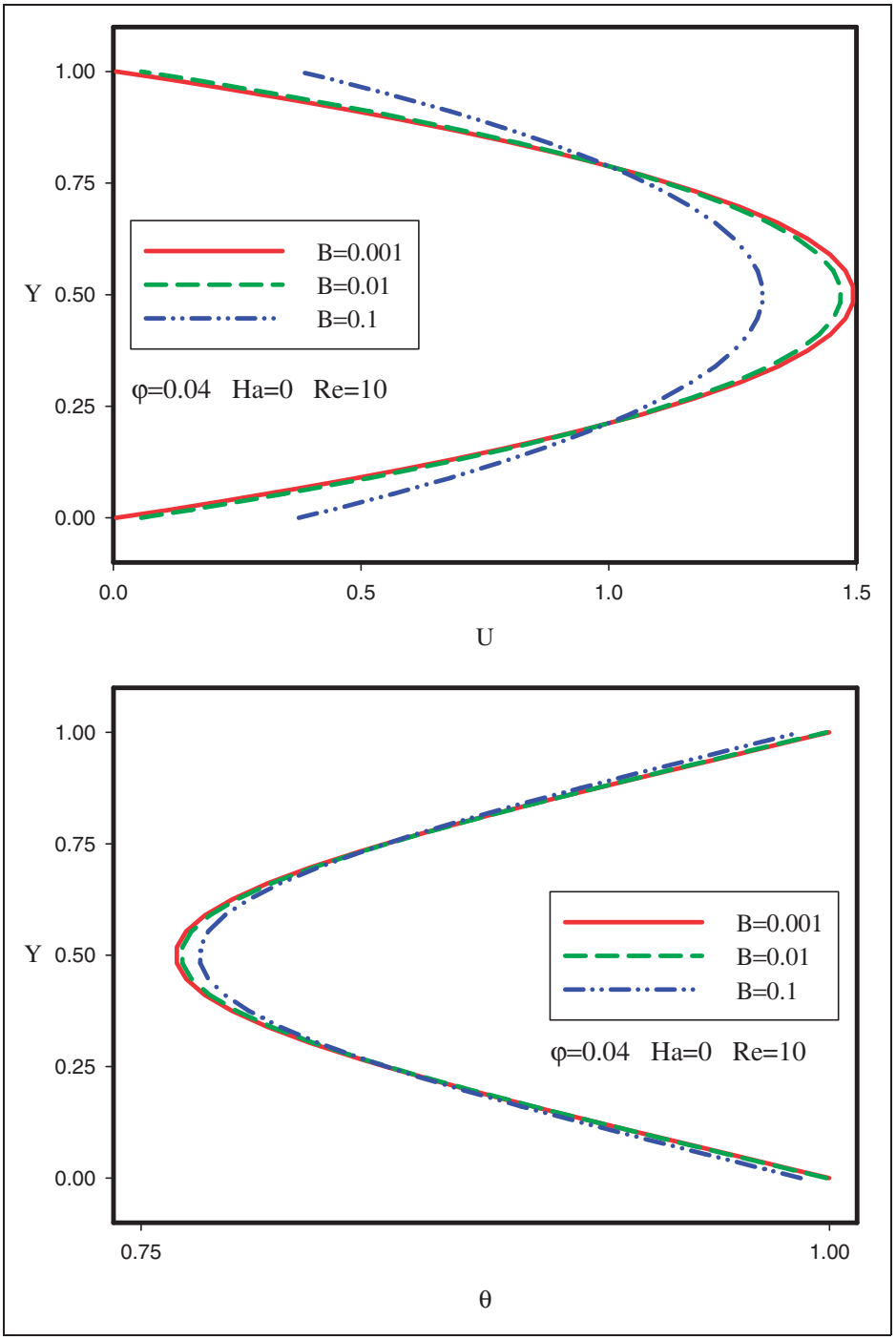

Figure 4. U and θ profiles of nanofluid at vertical centerline of microchannel ($X = L/2$) at $\varphi = 0.04$, $Ha = 0$, and $Re = 10$ for different values of B.

Effects of slip coefficient

Forced convection of water–Cu nanofluid in a two-dimensional horizontal microchannel is studied numerically. Microchannel domain is under the influence of a magnetic field with uniform strength of B_0 as shown in Figure 1. In addition, thermo-physical properties of copper (Cu) and water are presented in Table 3. Slip velocity (U_s) and temperature jump (θ_s) boundary conditions are considered along the microchannel walls for different values of slip coefficient such as $B = 0.001$, $B = 0.01$, and $B = 0.1$.

Figure 4 shows the horizontal velocity profiles (U) and temperature profiles (θ) at vertical centerline of microchannel ($X = L/2$) at $\varphi = 0.04$, $Ha = 0$, and $Re = 10$ for different values of B. It is observed that slip coefficient has significant effect on velocity profiles especially for $B = 0.1$. In the last case, slip velocity at

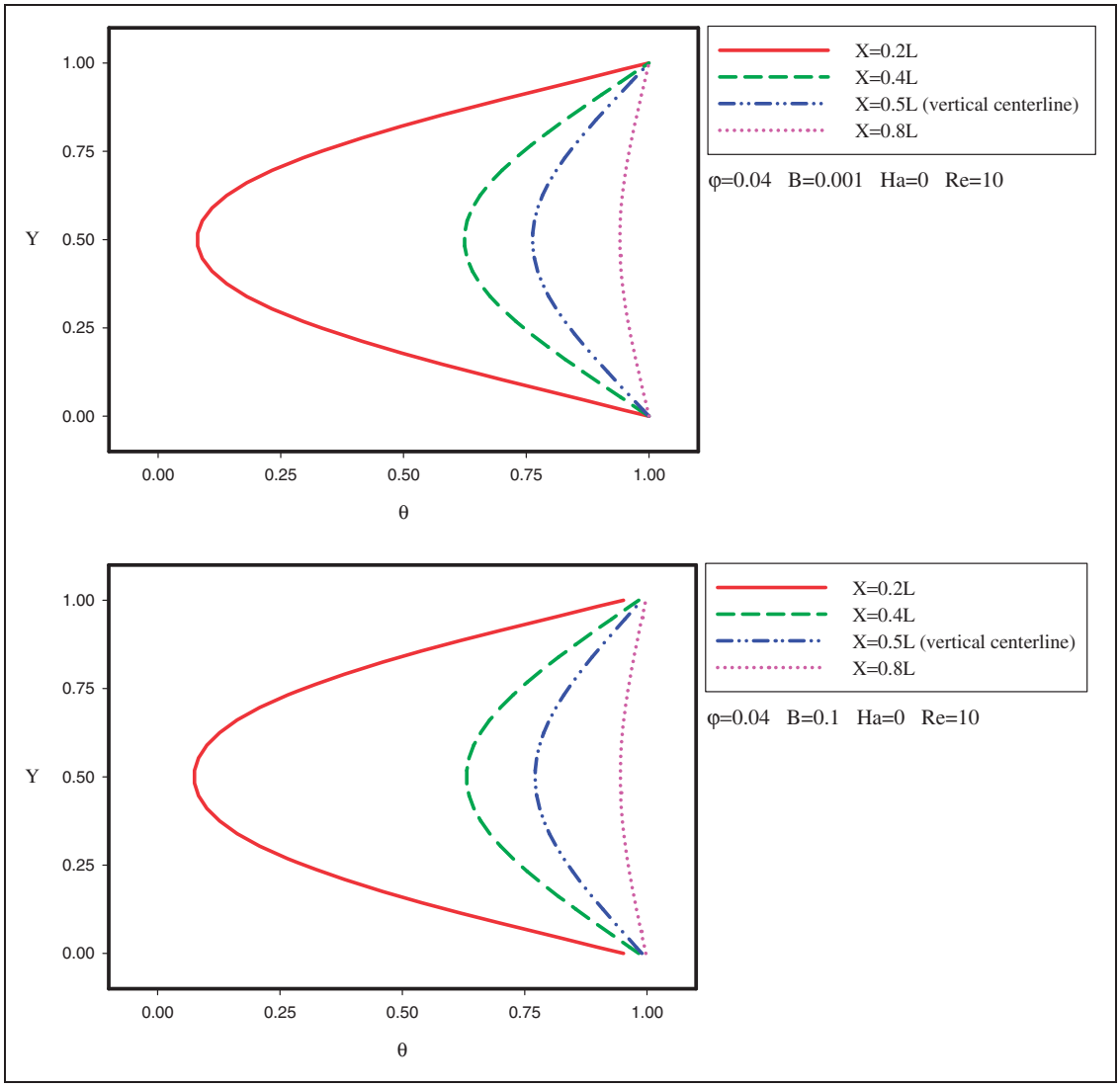

Figure 5. Dimensionless temperature profiles, θ, at different cross sections of microchannel at $\varphi = 0.04$, $Ha = 0$, and $Re = 10$ for different values of B.

$Y = 0$ and $Y = 1$ is almost equal to 0.37 and the maximum value of U is less than 1.5. Slip velocity existence adjacent to the wall leads to the decrease in the maximum value of U at $Y = 0.5$ to satisfy the continuity equation. Another significant effect of slip velocity would be generating the temperature jump along the walls, which can be seen in Figure 4. Fluid dimensionless temperate at $Y = 0$ and $Y = 1$ is 0.98 for the state of $B = 0.1$, which implies that temperature jump value (see equation (20) and the line after it) equals to $1 - 0.99 = 0.01$. The velocity profiles of $B = 0.001$ and $B = 0.01$ are more similar to one another in comparison with those of $B = 0.1$; this fact could also be seen in temperature profiles.

More discussion of temperature domain, dimensionless temperature profiles, θ, at different cross sections of microchannel at $\varphi = 0.04$, $Ha = 0$, and $Re = 10$ for $B = 0.001$ and $B = 0.1$ are shown in Figure 5. Nanofluid temperature increases along the microchannel length as well as at $X = 0.8L$ and its temperature tends to that of the wall. Moreover, the variations of temperature jump with X are clearly shown in this figure for $B = 0.1$ at $Y = 0$ and $Y = 1$. The highest amount of temperature jump is achieved at entrance region ($X = 0.2L$) which equals to $1 - 0.95 = 0.05$, then it begins to decrease with X, so that temperature jump would be equal to $1 - 0.99 = 0.01$ at $X = 0.5L$ (vertical centerline) and $X = 0.8L$. It should be mentioned that temperature jump was ignored in most of the previous works; however, this figure shows that its effects are significant in entrance region of the microchannel.

Effects of Hartmann number

Figure 6 indicates U profiles along the vertical centerline of microchannel at $Ha = 0$, $Ha = 15$, and $Ha = 30$

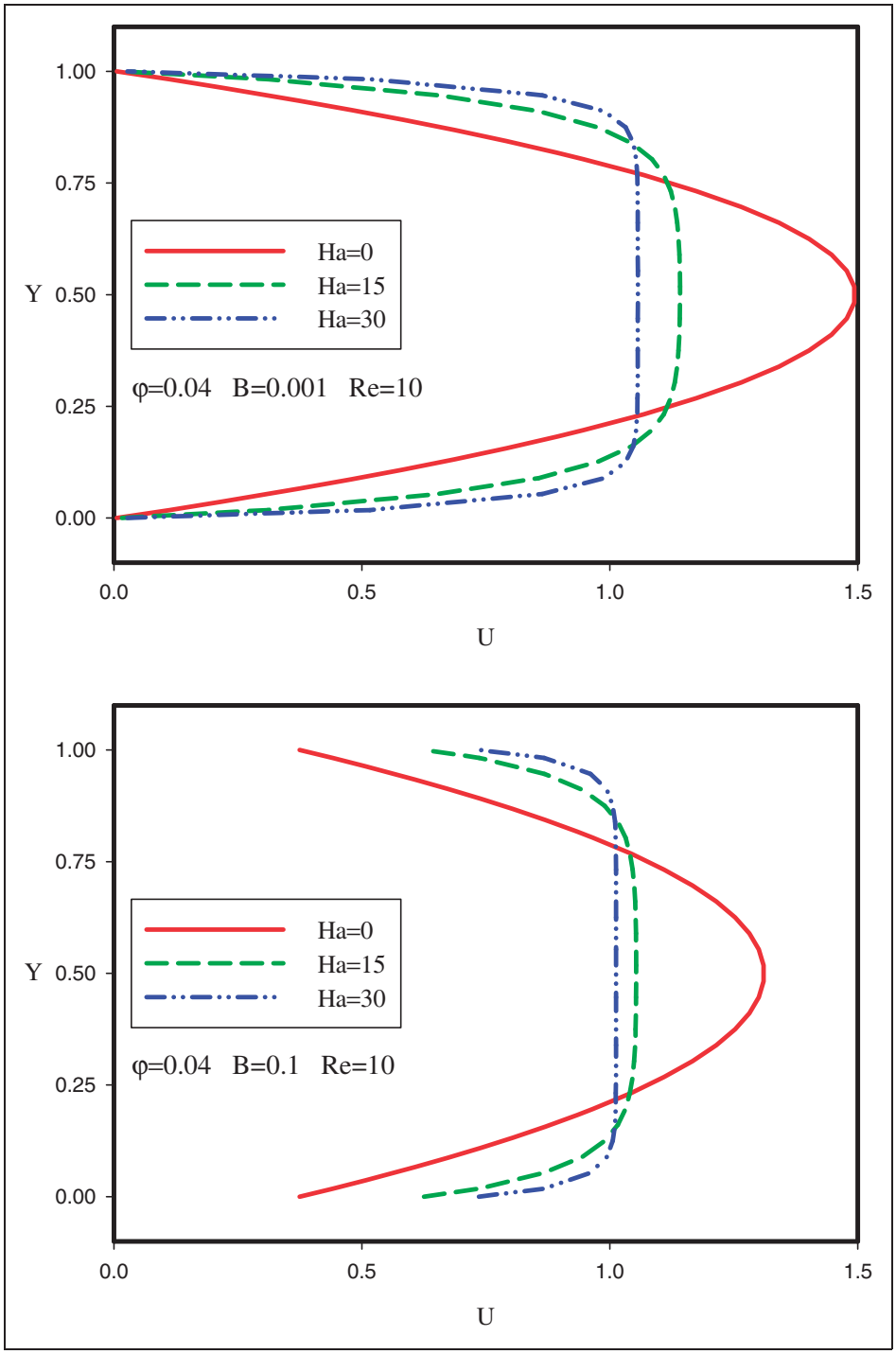

Figure 6. Dimensionless horizontal velocity profiles, U, at microchannel vertical centerline at different Ha's for $\varphi = 0.04$, $Re = 10$, $B = 0.001$, and $B = 0.1$.

for $\varphi = 0.04$, $Re = 10$, $B = 0.001$, and $B = 0.1$, respectively. Magnetic field existence leads to the generation of the Lorentz force in the opposite direction of X. Hence, more Ha corresponds to less maximum of U at horizontal centerline ($Y = 0.5$) and higher fluid velocity adjacent to the walls. As a result, the fully developed velocity profile would change with Ha. This fact can be traced well in Figure 6 at $B = 0.001$; so that stronger magnetic field corresponds to thinner boundary layer along the walls. Moreover, the thickness growth of the boundary layer is low at higher values of Ha.

The variation of slip velocity with Hartmann number is another interesting result of Figure 6 at $B = 0.1$. According to this figure, magnetic field affects the slip velocity on the walls so that higher Ha corresponds to higher amount of U_s. As it is said before, slip velocity is equal to 0.37 for $Ha = 0$ while it would

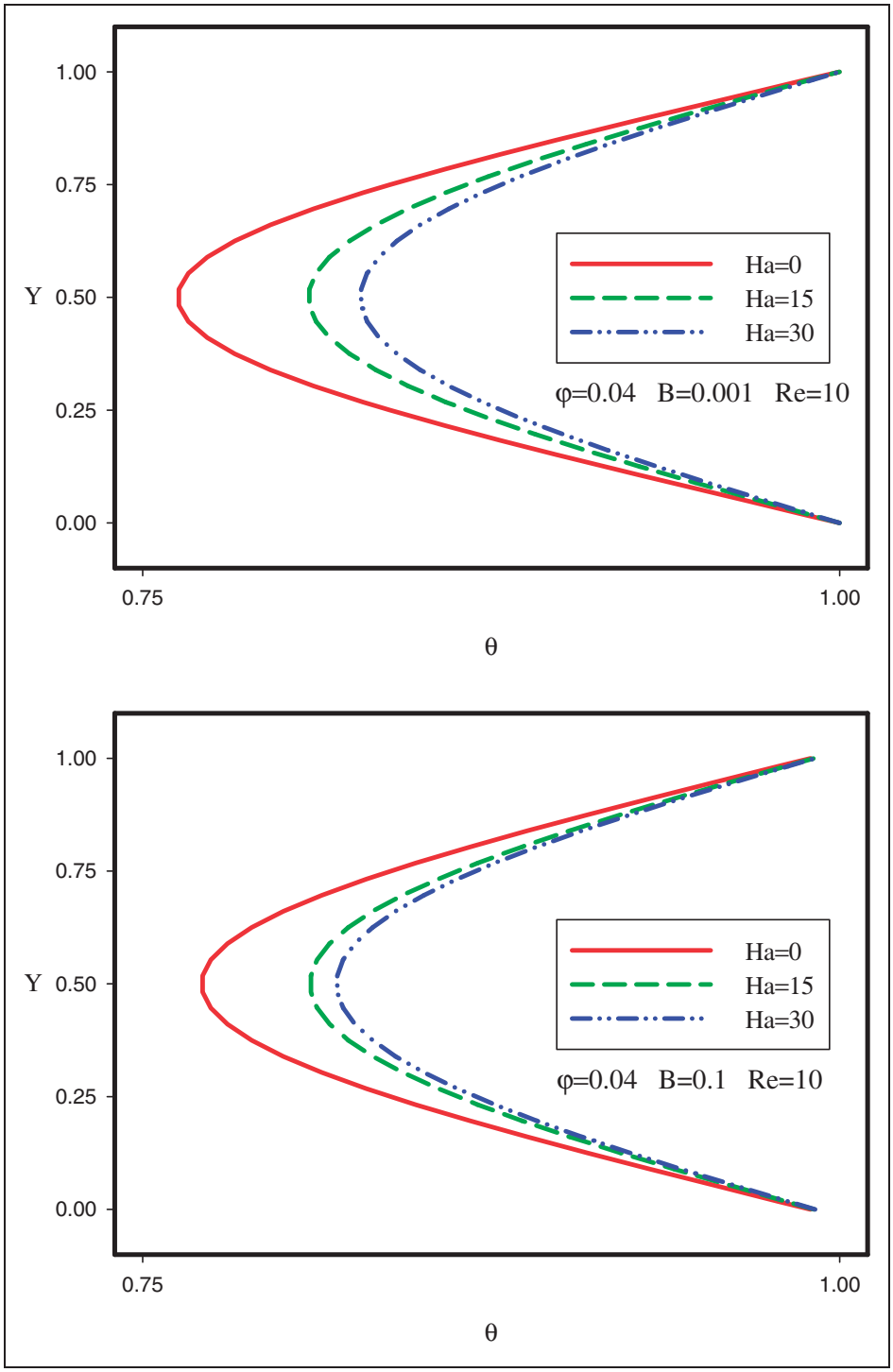

Figure 7. θ profiles at microchannel vertical centerline at different *Ha*'s for $\varphi = 0.04$, $Re = 10$, $B = 0.001$, and $B = 0.1$.

be 0.62 and 0.74 for $Ha = 15$ and $Ha = 30$, respectively.

Temperature profiles at microchannel vertical centerline at different *Ha*'s for $\varphi = 0.04$, $Re = 10$, $B = 0.001$, and $B = 0.1$ are presented in Figure 7 in order to show the effects of *Ha* on θ profiles. In spite of Figure 6, the plots of $B = 0.001$ and $B = 0.1$ in Figure 7 are almost similar to each other, which imply the insignificant effects of *B* and significant effects of *Ha* on temperature profiles, respectively. It is also observed that the fluid temperature in the middle of the microchannel ($Y = 0.5$) increases and tends to the wall's one at higher values of *Ha*. This fact implies more heat transfer existences due to more fluid velocity adjacent to the walls for the state of stronger magnetic field. Figure 8 shows the isotherms at $\varphi = 0.04$, $B = 0.1$, and $Ha = 30$ for $Re = 10$ and $Re = 50$. This figure represents a good visual aspect of nanofluid flow through the microchannel.

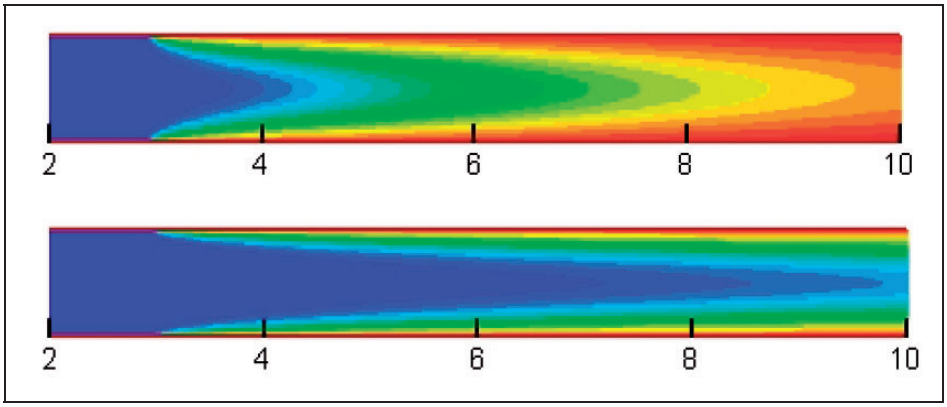

Figure 8. Isotherms at $\varphi = 0.04$, $B = 0.1$, and $Ha = 30$ for $Re = 10$ (top) and $Re = 50$ (bottom).

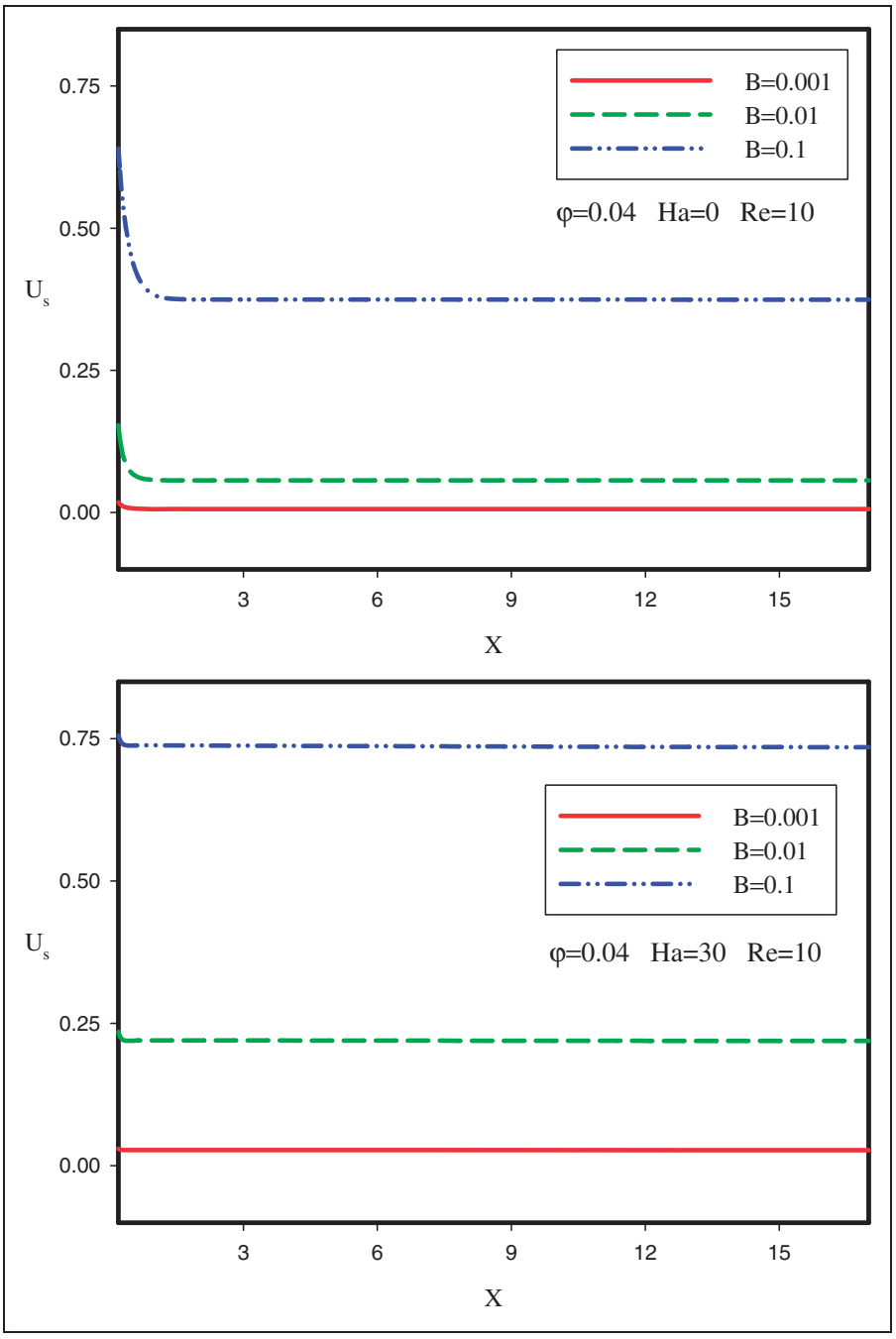

Figure 9. Slip velocity, U_s, along the microchannel wall at different values of B for $\varphi = 0.04$, $Re = 10$ at $Ha = 0$ and $Ha = 30$.

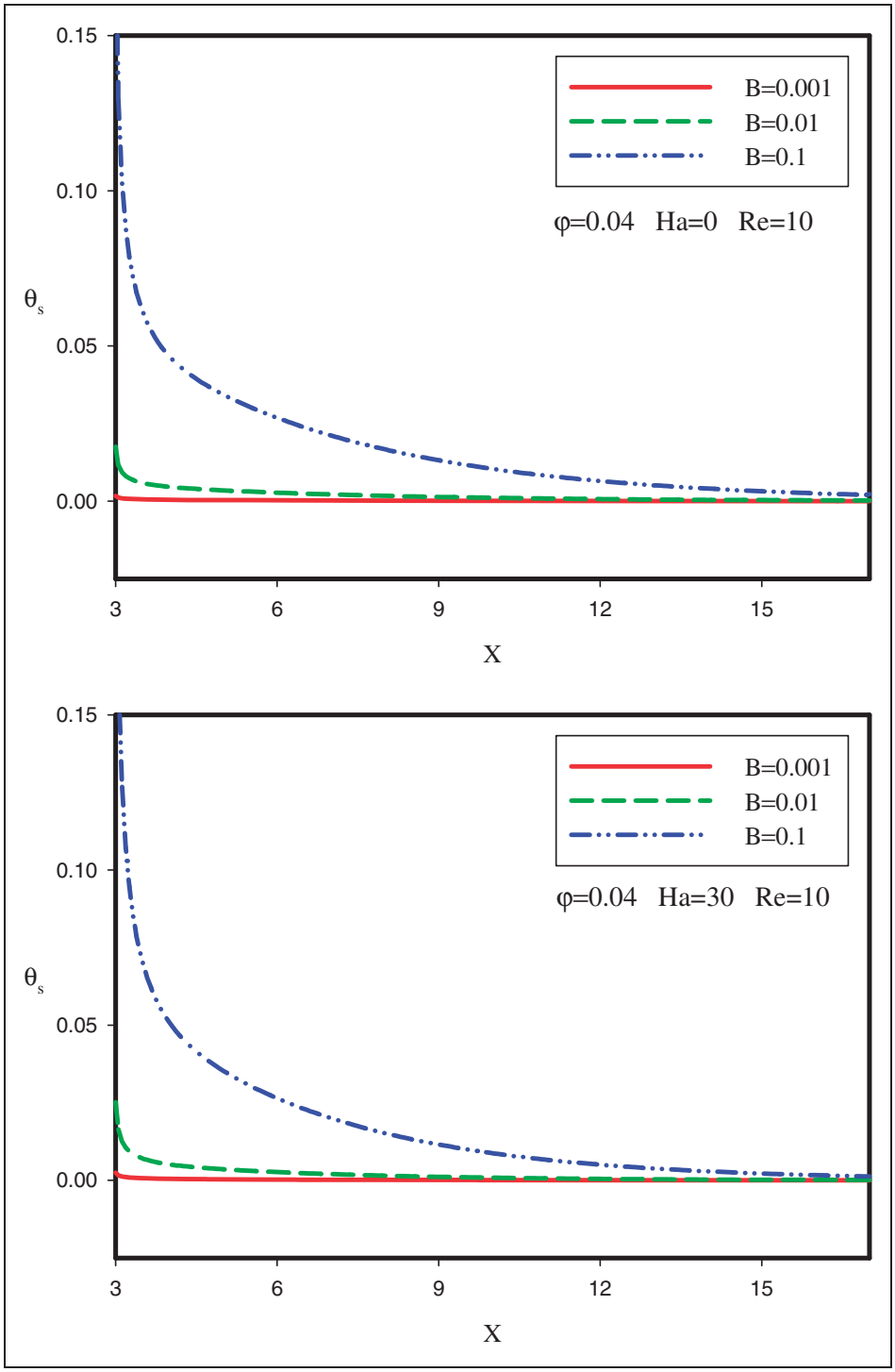

Figure 10. Temperature jump, θ_s, along the microchannel wall at different values of B for $\varphi = 0.04$, $Re = 10$ at $Ha = 0$ and $Ha = 30$.

Effects of Re, B, and Ha

Figure 9 shows the slip velocity, U_s, along the microchannel wall at different values of B for $\varphi = 0.04$, $Re = 10$ at $Ha = 0$ and $Ha = 30$. U_s starts from its maximum value at inlet and then it mildly decreases with X and, finally, approaches to a constant value along the wall. Moreover, slip coefficient has the significant increasing effect on it; however, this event could be severely invigorated for more Ha. The enhancing effect of magnetic field strength on slip velocity is shown for the first time in present work, which makes significantly higher shear stress on the walls. The positive effect of slip coefficient on temperature jump could also be seen in Figure 10 so that θ_s has its maximum amount at inlet and then approaches to the constant one along the wall. The comparison of these figure's plots of

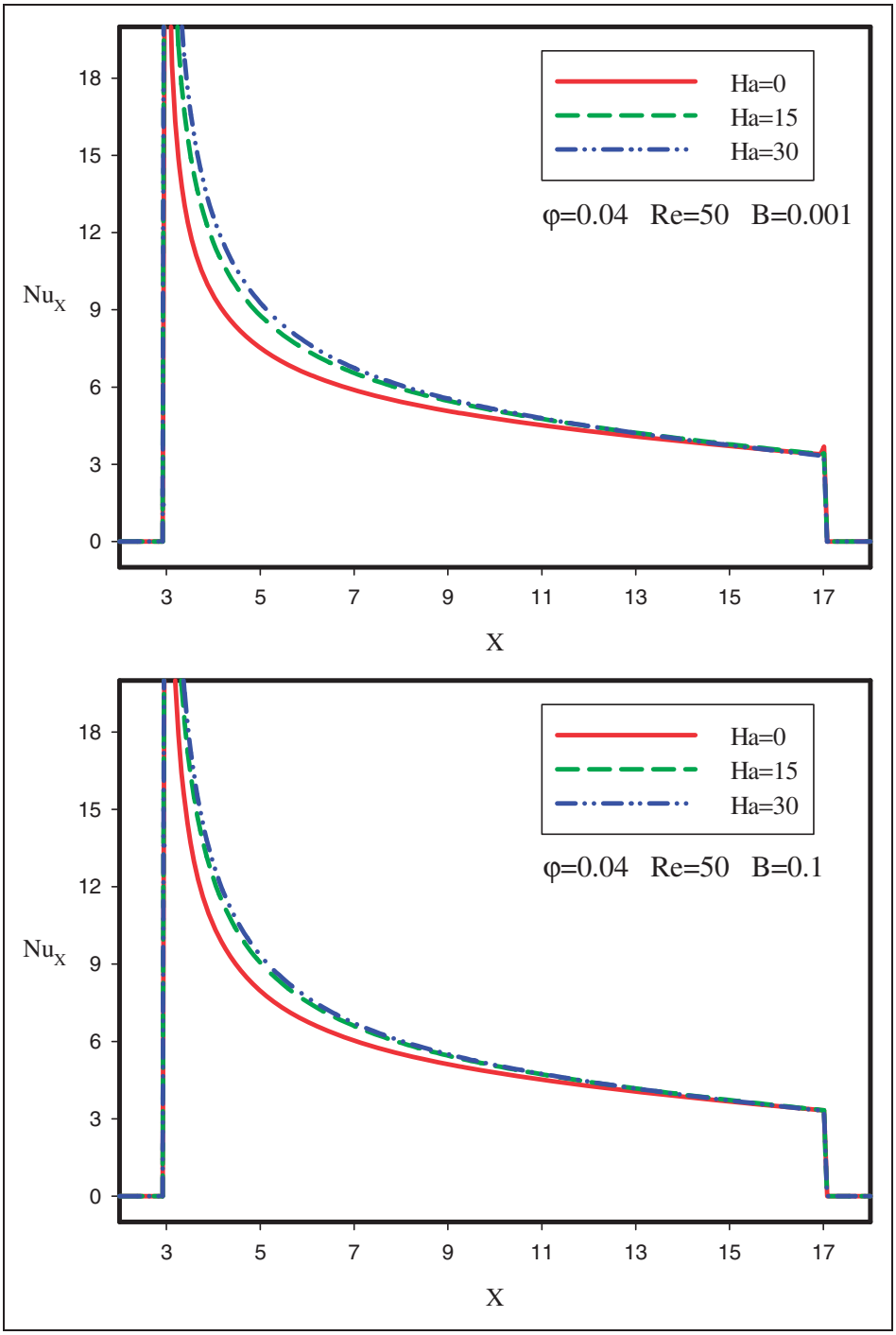

Figure 11. Nu_X along the microchannel wall at different values of Ha for $\varphi = 0.04$, $Re = 50$ at $B = 0.001$ and $B = 0.1$.

$Ha = 0$ and $Ha = 30$ imply the insignificant effects of Ha on θ_s.

Variations of local Nusselt number, Nu_X, along the microchannel wall at different values of Ha for $\varphi = 0.04$, $Re = 50$ at $B = 0.001$ and $B = 0.1$ are presented in Figure 11 to more tangible study of microchannel heat transfer. Higher Reynolds number leads to more heat transfer rate from the walls; so at this stage the value of Re is chosen to be equal to 50 to present the incoming data more clearly. It is obvious that Nu would be zero on the insulated walls; so Nu_X starts from its maximum value at $X = 3$ (beginning of the hot middle wall) and then it mildly decreases with X until $X = 17$, where it approaches zero again.

It is well known that the averaged Nusselt number, Nu_m, is the best parameter to indicate the overall heat transfer rate. Hence, Nu_m values on the microchannel wall at different amounts of Ha, φ, and B for $Re = 10$, $Re = 50$, and $Re = 100$ are presented in Figure 12. The positive influence of slip coefficient on heat transfer

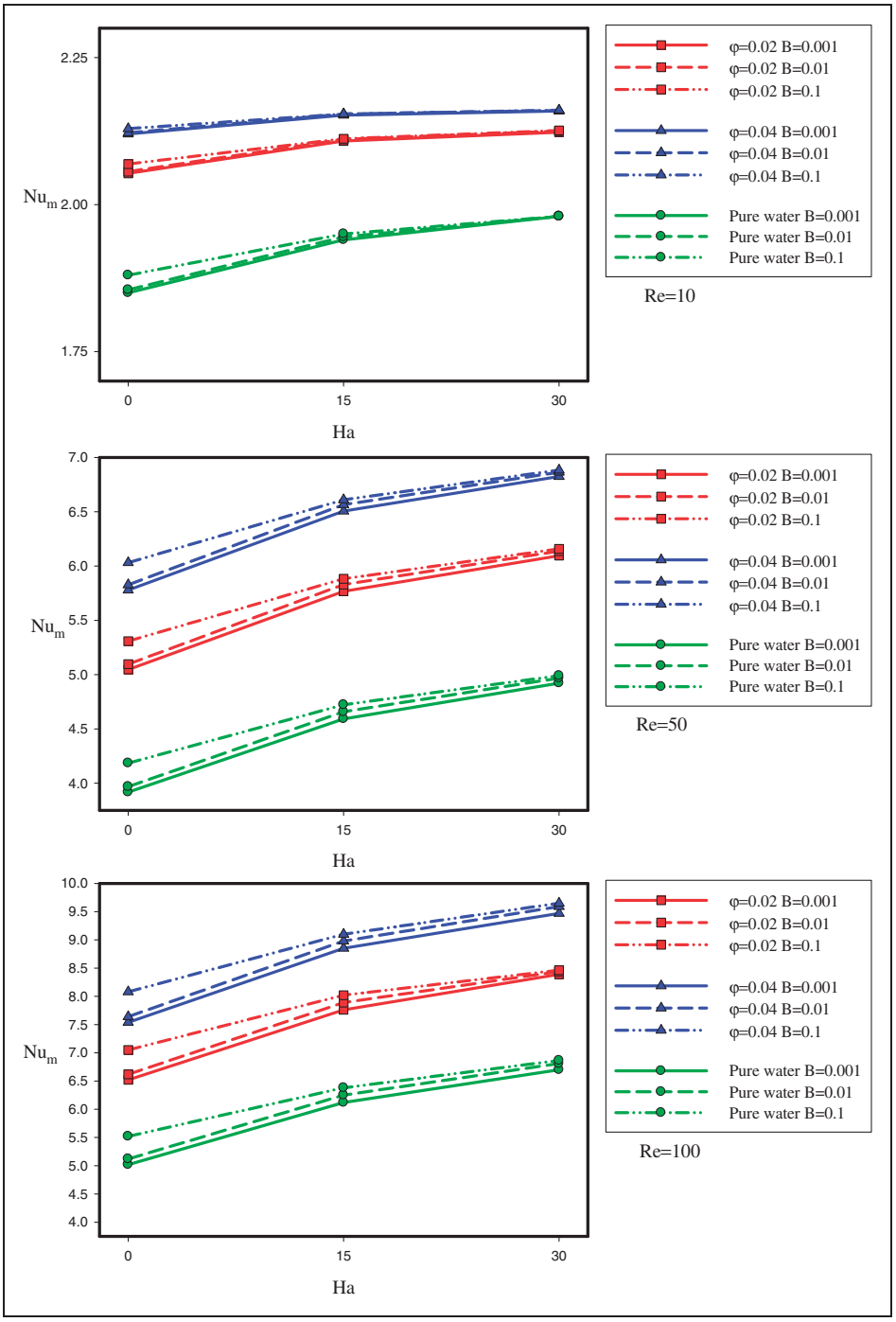

Figure 12. Nu_m on the microchannel wall at different values of Ha, φ, and B for $Re = 10$ (top), $Re = 50$ (middle), and $Re = 100$ (bottom).

rate in the absence of magnetic field can be traced well in this figure at $Ha = 0$, besides the enhancing effects of Re and φ on Nu_m. However, it is observed that the increase in Nusselt number by more slip coefficient at stronger magnetic field ($Ha = 30$) would be insignificant.

At last, it should be mentioned that the nanofluid Reynolds number and volume fraction cannot be increased simply in a microchannel. Hence, an alternative approach to increase Nu_m for the fixed value of B could be by using a greater magnetic field as well as higher Ha.

Conclusion

Forced convection of water–Cu nanofluid in a microchannel under the influence of the magnetic field is studied numerically. Slip velocity (U_s) and temperature jump (θ_s) boundary conditions are considered along the microchannel walls for different values of slip coefficient such as $B = 0.001$, $B = 0.01$, and $B = 0.1$. Hartmann number (Ha) is defined according to fluid properties to be consistent with definitions of Pr and Re; so the last term in right-hand side of equation (13) is developed.

Magnetic field existence leads to the generation of the Lorentz force in the opposite direction of X. Hence, higher Ha corresponds to less maximum of U at horizontal centerline and higher fluid velocity adjacent to the walls. As a result, the fully developed velocity profile would change with Ha. Moreover, nanofluid temperature increases along the microchannel as well as at $X = 0.8L$ and its temperature tends to that of the wall.

The effects of Hartmann number on slip velocity and temperature jump of nanofluid through the microchannel are studied for the first time in present work. U_s and θ_s start from their maximum values at inlet and then mildly decrease with X and finally approach to their related constant values along the walls. It is seen that higher Ha corresponds to higher U_s as well as slip velocity is equal to 0.37 for $Ha = 0$ (at $B = 0.1$) while it would be 0.62 and 0.74 for $Ha = 15$ and $Ha = 30$, respectively. However, the effects of Ha on θ_s would be negligible.

Larger slip coefficient increases slip velocity (U_s) and temperature jump (θ_s). However, this event could be severely invigorated at higher Ha as: $U_s = 0.05$ and $U_s = 0.22$ for $Ha = 0$ and $Ha = 30$ at $B = 0.01$; in comparison with $U_s = 0.37$ and $U_s = 0.74$ for $Ha = 0$ and $Ha = 30$ at $B = 0.1$.

Higher Reynolds number, slip coefficient, and volume fraction enhance the Nusselt number; however, the effect of slip coefficient (B) at higher amounts of magnetic field strength would be insignificant. Nevertheless, an alternative approach to increase Nu_m for the fixed value of B could be by using a greater magnetic field.

Acknowledgement

The authors of present article gratefully acknowledge the Research & Technology affairs of Najafabad Branch, Islamic Azad University, Isfahan, Iran, for the support in conducting this research work.

Declaration of Conflicting Interests

The author(s) declared no potential conflicts of interest with respect to the research, authorship, and/or publication of this article.

Funding

The author(s) received no financial support for the research, authorship, and/or publication of this article.

References

1. Lee S, Choi SUS, Li S, et al. Measuring thermal conductivity of fluids containing oxide nanoparticles. *ASME J Heat Transfer* 1999; 121: 280–289.
2. Eastman JA, Choi SUS, Yu W, et al. Anomalously increased effective thermal conductivity of ethylene glycol-based nanofluids containing copper nanoparticles. *Appl Phys Lett* 2001; 78: 718–720.
3. Das SK, Choi SUS, Yu W, et al. *Nanofluids: Science and technology*. Hoboken, NJ: Wiley Interscience, 2008.
4. Khanafer K, Vafai K and Lightstone M. Buoyancy-driven heat transfer enhancement in a two-dimensional enclosure utilizing nanofluids. *Int J Heat Mass Transfer* 2003; 46: 3639–3653.
5. Esfe MH, Esforjani SSM, Akbari M, et al. Mixed-convection flow in a liddriven square cavity filled with a nanofluid with variable properties: Effect of the nanoparticle diameter and of the position of a hot obstacle. *Heat Transfer Res* 2014; 45: 563–578.
6. Esfe MH, Arani AAA, Karimipour A, et al. Numerical simulation of natural convection around an obstacle placed in an enclosure filled with different types of nanofluids. *Heat Transfer Res* 2014; 45: 279–292.
7. Karimipour A, Mirtalebi SS, Afrand M, et al. Using nanofluid in lid driven shallow enclosure at particular Richardson number: Investigation the effect of velocity ratio. *Ind J Sci Technol* 2014; 7: 698–704.
8. Oztop HF and Abu-Nada E. Numerical study of natural convection in partially heated rectangular enclosures filled with nanofluids. *Int J Heat Fluid Flow* 2008; 29: 1326–1336.
9. Tiwari RK and Das MK. Heat transfer augmentation in a two-sided lid-driven differentially heated square cavity utilizing nanofluid. *Int J Heat Mass Transfer* 2007; 50: 2002–2018.
10. Goodarzi M, Safaei MR, Vafai K, et al. Investigation of nanofluid mixed convection in a shallow cavity using a two-phase mixture model. *Int J Therm Sci* 2014; 75: 204–220.
11. Karimipour A, Nezhad AH, Behzadmehr A, et al. Periodic mixed convection of a nanofluid in a cavity with top lid sinusoidal motion. *Proc IMechE, Part C: J Mechanical Engineering Science* 2011; 225: 2149–2160.
12. Karimipour A, Esfe MH, Safaei MR, et al. Mixed convection of copper–water nanofluid in a shallow inclined lid driven cavity using the lattice Boltzmann method. *Physica A* 2014; 402: 150–168.
13. Esfe MH, Akbari M, Toghraie D, et al. Effect of nanofluid variable properties on mixed convection flow and heat transfer in an inclined two-sided lid-driven cavity with sinusoidal heating on sidewalls. *Heat Transfer Res* 2014; 45: 409–432.
14. Akbarinia A and Behzadmehr A. Numerical study of laminar mixed convection of a nanofluid in horizontal curved tubes. *Appl Therm Eng* 2007; 27: 1327–1337.
15. Safaei MR, Mahian O, Garoosi F, et al. Investigation of micro- and nanosized particle erosion in a 90° pipe bend using a two-phase discrete phase model. *Scient World J* 2014. Article ID 740578, 12 pages, http://dx.doi.org/10.1155/2014/740578.
16. Behzadmehr A, Saffar-Avval M and Galanis N. Prediction of turbulent forced convection of a nanofluid in a tube with uniform heat flux using a two phase approach. *Int J Heat Fluid Flow* 2007; 28: 211–219.
17. Pishkar I and Ghasemi B. Cooling enhancement of two fins in a horizontal channel by nanofluid mixed convection. *Int J Therm Sci* 2012; 59: 141–151.
18. Santra AK, Sen S and Chakraborty N. Study of heat transfer due to laminar flow of copper–water nanofluid through two isothermally heated parallel plates. *Int J Therm Sci* 2009; 48: 391–400.
19. Gad-el-Hak M. Flow physics in MEMS. *Rev Mech Ind* 2001; 2: 313–341.
20. Karimipour A, Nezhad AH, D'Orazio A, et al. Simulation of copper–water nanofluid in a

microchannel in slip flow regime using the lattice Boltzmann method. *Eur J Mech B/Fluids* 2015; 49: 89–99.
21. Kavehpour HP, Faghri M and Asako Y. Effects of compressibility and rarefaction on gaseous flows in microchannels. *Numer Heat Transfer A* 1997; 32: 677–696.
22. Zahid WA, Yin Y and Zhu K. Couette-Poiseuille flow of a gas in long microchannels. *Microfluid Nanofluid* 2007; 3: 55–64.
23. Duan Z. Slip flow in doubly connected microchannels. *Int J Therm Sci* 2012; 58: 45–51.
24. Goodarzi M, Safaei MR, Karimipour A, et al. Comparison of the finite volume and lattice Boltzmann methods for solving natural convection heat transfer problems inside cavities and enclosures. *Abstract Appl Anal* 2014. Article ID 762184, 15 pages, http://dx.doi.org/10.1155/2014/762184.
25. Karimipour A, Afrand M, Akbari M, et al. Simulation of fluid flow and heat transfer in the inclined enclosure. *World Acad Sci Eng Technol* 2012; 61: 435–440.
26. Bird G. *Molecular gas dynamics and the direct simulation of gas flows*. Oxford: Oxford University Press, 1994.
27. Karimipour A, Nezhad AH, D'Orazio A, et al. The effects of inclination angle and Prandtl number on the mixed convection in the inclined lid driven cavity using lattice Boltzmann method. *J Theoret Appl Mech* 2013; 51: 447–462.
28. Karimipour A, Nezhad AH, D'Orazio A, et al. Investigation of the gravity effects on the mixed convection heat transfer in a microchannel using lattice Boltzmann method. *Int J Therm Sci* 2012; 54: 142–152.
29. Raisi A, Ghasemi B and Aminossadati SM. A numerical study on the forced convection of laminar nanofluid in a microchannel with both slip and no-slip conditions. *Numer Heat Transfer A* 2011; 59: 114–129.
30. Mital M. Analytical analysis of heat transfer and pumping power of laminar nanofluid developing flow in microchannels. *Appl Therm Eng* 2013; 50: 429–436.
31. Akbarinia A, Abdolzadeh M and Laur R. Critical investigation of heat transfer enhancement using nanofluids in microchannels with slip and non-slip flow regimes. *Appl Therm Eng* 2011; 31: 556–565.
32. Mah WH, Hung YM and Guo N. Entropy generation of viscous dissipative nanofluid flow in microchannels. *Int J Heat Mass Transfer* 2012; 55: 4169–4182.
33. Kalteh M, Abbassi A, Saffar-Avval M, et al. Eulerian–Eulerian two-phase numerical simulation of nanofluid laminar forced convection in a microchannel. *Int J Heat Fluid Flow* 2011; 32: 107–116.
34. Singh PK, Harikrishna PV, Sundararajan T, et al. Experimental and numerical investigation into the hydrodynamics of nanofluids in microchannels. *Exp Therm Fluid Sci* 2012; 42: 174–186.
35. Byrne MD, Hart RA and Silva AKd. Experimental thermal–hydraulic evaluation of CuO nanofluids in microchannels at various concentrations with and without suspension enhancers. *Int J Heat Mass Transfer* 2012; 55: 2684–2691.
36. Yang YT and Lai FH. Numerical study of flow and heat transfer characteristics of alumina-water nanofluids in a microchannel using the lattice Boltzmann method. *Int Commun Heat Mass Transfer* 2011; 38: 607–614.
37. Ellahi R. The effects of MHD and temperature dependent viscosity on the flow of non-Newtonian nanofluid in a pipe: Analytical solutions. *Appl Math Model* 2013; 37: 1451–1467.
38. Ghasemi B, Aminossadati SM and Raisi A. Magnetic field effect on natural convection in a nanofluid-filled square enclosure. *Int J Therm Sci* 2011; 50: 1748–1756.
39. Sheikholeslami M, Gorji-Bandpy M, Ganji DD, et al. Natural convection of nanofluids in an enclosure between a circular and a sinusoidal cylinder in the presence of magnetic field. *Int Commun Heat Mass Transfer* 2012; 39: 1435–1443.
40. Zheng L, Niu J, Zhang X, et al. MHD flow and heat transfer over a porous shrinking surface with velocity slip and temperature jump. *Math Comput Model* 2012; 56: 133–144.
41. Turkyilmazoglu M. Exact analytical solutions for heat and mass transfer of MHD slipflow in nanofluids. *Chem Eng Sci* 2012; 84: 182–187.
42. Aminossadati SM, Raisi A and Ghasemi B. Effects of magnetic field on nanofluid forced convection in a partially heated microchannel. *Int J Nonlinear Mech* 2011; 46: 1373–1382.
43. Mahmoudi AH, Pop I and Shahi M. Effect of magnetic field on natural convection in a triangular enclosure filled with nanofluid. *Int J Therm Sci* 2012; 59: 126–140.
44. Xuan Y and Li Q. Investigation on convective heat transfer and flow features of nanofluids. *ASME J Heat Transfer* 2003; 125: 151–155.
45. Chon CH, Kihm KD, Lee SP, et al. Empirical correlation finding the role of temperature and particle size for nanofluid (AL_2O_3) thermal conductivity enhancement. *Appl Phys Lett* 2005; 87: 1–3.
46. Maxwell JC. *A treatise on electricity and magnetism*. 2nd ed. Cambridge: Oxford University Press, 1904, pp.435–441.
47. Thompson PA and Troian SM. A general boundary condition for liquid flow at solid surfaces. *Phys Rev Lett* 1997; 63: 766–769.
48. Ngoma GD and Erchiqui F. Heat flux and slip effects on liquid flow in a microchannel. *Int J Therm Sci* 2007; 46: 1076–1083.
49. Zhang YH, Qin RS, Sun YH, et al. Gas flow in microchannels - A lattice Boltzmann method approach. *J Stat Phys* 2005; 121: 257–267.

Appendix

Notation

AR	microchannel aspect ratio ($=L/H$)
B	nondimensional slip coefficient ($=\beta/h$)
B_0	magnetic field strength
B_c	Boltzman constant ($=1.3807 \times 10^{-23}$ J/K)
c_p	specific heat (J/kgK)
d_f	molecular diameter of base fluid (nm)
d_p	nanoparticles diameter ($=10$ nm)
h	microchannel height (m)
H	nondimensional microchannel height
Ha	Hartmann number ($=B_0 h(\sigma_f/\mu_f)^{0.5}$)
k	thermal conductivity (W/mK)

l	microchannel length (m)
L	nondimensional microchannel length (m)
L_{BF}	mean free path of base fluid (nm)
Nu	Nusselt number
p	pressure (Pa)
P	nondimensional pressure
Pr	Prandtl number ($=\upsilon_f/\alpha_f$)
Re	Reynolds number ($=u_i h/\upsilon_f$)
T	temperature (K)
T_C	temperature of cold inlet nanofluid (K)
T_H	temperature of hot walls (K)
u	horizontal velocity (m/s)
u_i	nanofluid inlet velocity (m/s)
U	nondimensional horizontal velocity
U_s	nondimensional slip velocity
v	vertical velocity (m/s)
V	nondimensional vertical velocity
x	horizontal Cartesian coordinate (m)
X	nondimensional horizontal Cartesian coordinate
y	vertical Cartesian coordinate (m)
Y	nondimensional vertical Cartesian coordinate
α	thermal diffusivity ($=k/\rho c_p$ m^2/s)
β	slip coefficient (m)
μ	dynamic viscosity (Ns/m^2)
φ	volume fraction of nanoparticles
σ	electrical conductivity (S/m)
θ	nondimensional temperature
θ_s	nondimensional temperature jump
ρ	density (kg/m^3)
υ	kinematic viscosity (m^2/s)

Subscripts

eff	effective
f	fluid
m	averaged value
nf	nanofluid
s	solid
x	local value in X-direction